# Stable and Accurate Boundary Conditions for Aerodynamic and Aeroacoustic Calculations

Gunilla Kreiss, Malin Siklosi, Christer Johansson, Mattias Liefvendahl Nada, the Department of Numerical Analysis and Computer Science, the Royal Institute of Technology, Stockholm

and

Jan Nordström FFA, the Aeronautical Research Institute of Sweden and the Department of Scientific Computing, Uppsala University

August 28, 2000

#### Abstract

Boundary conditions leading to small errors in the continuous problem can make the construction of a stable and accurate discrete scheme very difficult. We discuss this problem and focus on the common procedure of specifying the pressure at a subsonic outflow boundary. The result of the analysis provide numerical boundary conditions for both inflow and outflow boundaries that lead to second order accurate results. Numerical experiments that support the theoretical conclusions are presented.

### 1 Introduction

Although computational fluid dynamics (CFD) has had a great impact on aerospace engineering, this impact has mainly been limited to steady flows, such as the flow around a cruising aircraft. The jump to truly dynamic problems, caused for example by gusts, other passing aircrafts, flight maneuvers, propellers and moving or deforming control surfaces is highly nontrivial, and leads to a number of new difficulties. Chief among these are the development of accurate time-dependent boundary conditions at artificial boundaries.

Accurate time-dependent boundary conditions is also of the utmost importance is computational aeroacoustics. The nonlinear sound source is often computed using conventional CFD methods (finite volume in space and Runge-Kutta in time, see [7]). The outer linear acoustic problem can be solved using for example the so called Kirchhof method [6] where the CFD solution is used as boundary data on a cylinder surface surrounding the source. An accurate noise prediction require accurate boundary data, which in turn means accurate far field boundary conditions in the CFD calculation.

To obtain accurate solutions in the numerical calculation, well-posed boundary conditions with accurate data are required. In [5][4], it is shown that if one measure the influence of a small error introduced at a farfield boundary in a *local norm*, it decreases with increasing distance to the boundary. The discretized problem (including the discrete version of the well posed boundary conditions) must be augmented with numerical boundary conditions such that a stable and sufficiently accurate discrete solution is obtained. The numerical boundary conditions can be at most one order less accurate than the scheme in the interior, see [1] [2].

Sometimes, and this is the topic of this paper, a conflict between the mathematical boundary condition and the numerical boundary conditions appears. An optimal boundary condition leading to a small error in the continuous problem can make the construction of a stable and accurate discrete scheme very difficult. In this paper we will discuss this problem and focus on the common procedure of specifying the pressure (leads to a well posed problem and the error in the data is often small) at a subsonic outflow boundary. The analysis presented in this paper is for the corresponding semi-discrete quater-space problem,  $(x \geq 0, t \geq 0)$ , linearized at a constant subsonic state.

# 2 Euler equations

The Euler equations for a polytropic gas in one space dimension are

$$\tilde{\rho}_t + (\tilde{\rho}u)_x = 0 \tag{1a}$$

$$\tilde{u}_t + \tilde{u}\tilde{u}_x + \frac{1}{\tilde{\rho}}\tilde{p}_x = 0 \tag{1b}$$

$$\tilde{p}_t + \tilde{u}\tilde{p}_x + \gamma \tilde{p}\tilde{u}_x = 0. \tag{1c}$$

Here  $\tilde{\rho}$  is the density,  $\tilde{u}$  the velocity,  $\tilde{p}$  the pressure and  $\gamma$  is the ratio of specific heat. The speed of sound is  $c=\sqrt{\frac{\gamma \tilde{p}}{\tilde{\rho}}}$ . In order to have a well defined solution in the region  $x\geq 0,\,t\geq 0$  we need initial conditions

$$\tilde{u}(x,0) = u_0(x), \quad \tilde{\rho}(x,0) = \rho_0(x), \quad \tilde{p}(x,0) = p_0(x),$$
 (2)

and boundary conditions at x=0. In the case of subsonic outflow one boundary condition should be prescribed since one characteristic enters the domain. We will consider

$$\tilde{p}(0,t) = g(t). \tag{3}$$

Linearizing (1) at a constant subsonic state (R, U, P) yields

$$\begin{pmatrix} \tilde{\rho} \\ \tilde{u} \\ \tilde{p} \end{pmatrix}_t + \begin{pmatrix} U & R & 0 \\ 0 & U & R^{-1} \\ 0 & \gamma P & U \end{pmatrix} \begin{pmatrix} \tilde{\rho} \\ \tilde{u} \\ \tilde{p} \end{pmatrix}_x = 0. \tag{4}$$

The initial and boundary conditions are of the same form as before.

Note that  $\tilde{u}$  and  $\tilde{p}$  are independent of  $\tilde{\rho}$ . In this paper we only consider numerical boundary conditions that do not couple  $\tilde{u}$  and  $\tilde{p}$  to  $\tilde{\rho}$ . Thus it suffices to analyze

$$\begin{pmatrix} \tilde{u} \\ \tilde{p} \end{pmatrix}_t + \begin{pmatrix} U & R^{-1} \\ \gamma P & U \end{pmatrix} \begin{pmatrix} \tilde{u} \\ \tilde{p} \end{pmatrix}_x = 0. \tag{5}$$

Below we will comment on how to apply our results to the full system.

Introduce the scaling

$$\begin{pmatrix} \tilde{u} \\ \tilde{p} \end{pmatrix} = \begin{pmatrix} u \\ \sqrt{\gamma RP} p \end{pmatrix}, \quad x = C\tilde{x}, \quad C = \sqrt{\frac{\gamma P}{R}}, \tag{6}$$

yielding

$$\begin{pmatrix} u \\ p \end{pmatrix}_t + \begin{pmatrix} m & 1 \\ 1 & m \end{pmatrix} \begin{pmatrix} u \\ p \end{pmatrix}_x = 0, \quad m = \frac{U}{C}, \quad -1 < m < 1. \tag{7}$$

A corresponding semi-discrete problem is obtained by introducing gridpoints  $x_i = ih - h/2$ , i = 1, 2, ..., and corresponding gridfunctions  $u_i, p_i, i = 0, 1, ...$  The space derivatives are replaced by central differences,

$$\begin{pmatrix} u_i \\ p_i \end{pmatrix}_t = -\frac{1}{2h} \begin{pmatrix} m & 1 \\ 1 & m \end{pmatrix} \begin{pmatrix} u_{i+1} - u_{i-1} \\ p_{i+1} - p_{i-1} \end{pmatrix}$$
(8)

The boundary condition (3) is replaced by

$$p_0 + p_1 = 2g(t). (9)$$

The semi-discrete problem will not have a well defined solution unless a numerical boundary condition is added at x=0 and we require  $||u||_h + ||p||_h < \infty$ . We define a discrete scalar product and norm by

$$(u,v)_h = \sum_{i=1}^{\infty} \langle u_i, v_i \rangle h, \quad ||u||_h^2 = (u,u)_h, \quad \langle u_i, v_i \rangle = \bar{u}_i v_i. \tag{10}$$

We will investigate two different possibilities for the numerical boundary condition at x = 0.

Case 1. The primitive variable u is extrapolated,

$$u_0 - 2u_1 + u_2 = 0. (11)$$

The boundary conditions (9) and (11) can be written on the more compact matrix form

$$L_1 \begin{pmatrix} u_0 \\ p_0 \end{pmatrix} = G_1, \tag{12}$$

where

$$L_1 = \begin{pmatrix} (1-E)^2 & 0 \\ 0 & 1+E \end{pmatrix}, \quad G_1 = \begin{pmatrix} 0 \\ 2g(t) \end{pmatrix},$$

and the translation operator E is defined as

$$(Ev)_i = v_{i+1}.$$

Case 2. The outgoing characteristic variable u-p is extrapolated,

$$u_0 - p_0 - 2(u_1 - p_1) + u_2 - p_2 = 0. (13)$$

In matrix form (9) and (13) are

$$L_2 \begin{pmatrix} u_0 \\ p_0 \end{pmatrix} = G_2, \tag{14}$$

where

$$L_2 = \begin{pmatrix} (1-E)^2 & -(1-E)^2 \\ 0 & 1+E \end{pmatrix}, \quad G_2 = \begin{pmatrix} 0 \\ 2g(t) \end{pmatrix}.$$

# 3 Conditions for Stability

In this section we will use the Laplace transform technique described in [3] to investigate the stability of the semi-discrete problem. First we prove a theorem relating the stability of (8) together with boundary conditions of the form

$$L\begin{pmatrix} u_0 \\ p_0 \end{pmatrix} = G \tag{15}$$

to an algebraic condition. With the help of this theorem we investigate the stability of (8) with boundary conditions (12) or (14). To conclude the section we prove that in the case of boundary condition (14) the numerical solution is second order accurate.

To simplify the analysis, we introduce the characteristic variables

$$v_i = \begin{pmatrix} \overline{u}_i \\ \overline{p}_i \end{pmatrix} \equiv S^{-1} \begin{pmatrix} u_i \\ p_i \end{pmatrix}, \quad S = \begin{pmatrix} -1 & 1 \\ 1 & 1 \end{pmatrix}.$$
 (16)

With these variables the matrix in equation (8) is transformed to

$$S^{-1} \begin{pmatrix} m & 1 \\ 1 & m \end{pmatrix} S = \begin{pmatrix} \lambda_1 & 0 \\ 0 & \lambda_2 \end{pmatrix} \equiv \Lambda, \tag{17}$$

where  $\lambda_1 = m - 1$  and  $\lambda_2 = m + 1$ .

Define

$$Q \equiv -\Lambda(E - E^{-1}) \tag{18}$$

then the (8) with boundary condition can be written as

$$\frac{d_i}{dt} = \frac{1}{2h}Qv_i + F_i,\tag{19a}$$

$$LSv_0 = G, \quad ||v||_h < \infty, \tag{19b}$$

$$v_i(0) = f_i, \quad i = 0, 1, \dots$$
 (19c)

Here we have included a forcing F in the equation.

### 3.1 Sufficient Conditions for Stability

In this subsection we investigate what conditions on L are sufficient for (19) to be strongly stable.

Consider the two auxiliary problems:

$$\frac{dw_i}{dt} = \frac{1}{2h}Qw_i + F_i,\tag{20a}$$

$$w_i(0) = f_i, (20b)$$

$$\tilde{L}w_0 \equiv \begin{pmatrix} w_0^{(1)} - w_1^{(1)} \\ w_0^{(2)} + w_1^{(2)} \end{pmatrix} = 0, \quad ||w||_h < \infty,$$
(20c)

and

$$\frac{dy_i}{dt} = \frac{1}{2h}Qy_i,\tag{21a}$$

$$y_i(0) = 0, (21b)$$

$$LSy_0 = G - LSw_0 \equiv \tilde{G}, \quad ||y||_h < \infty. \tag{21c}$$

We assume that the boundary condition in equation (21) can be expressed as

$$y_0 = \sum_{j=1}^{q} B_j y_j + B_0 \tilde{G}, \tag{22}$$

where  $B_j, j = 0, 1, ..., q$ , are bounded matrices and independent of h. We see that  $v_i = w_i + y_i$  satisfies (19).

Lemma 1 The solution of system (20) satisfies

$$||w(t)||_{h}^{2} + C \int_{0}^{t} (|w_{0}|^{2} + |w_{1}|^{2}) d\tau \le 2||f||_{h}^{2} + 2 \int_{0}^{t} ||F(\tau)||_{h}^{2} d\tau, \tag{23}$$

where C > 0 is a constant.

Proof.

A standard energy estimate gives

$$\begin{aligned} \frac{d}{dt}||w||_{h}^{2} &= (-\Lambda D_{0}w, w)_{h} + (w, -\Lambda D_{0}w)_{h} + (w, F)_{h} + (F, w)_{h} \\ &= (-\Lambda D_{0}w, w)_{h} - (-\Lambda D_{0}w, w)_{h} - \frac{1}{2}(\overline{w}_{j}\Lambda w_{j+1} + \overline{w}_{j+1}\Lambda w_{j})\Big|_{0}^{\infty} \\ &+ (w, F)_{h} + (F, w)_{h}, \end{aligned}$$

where  $\Lambda D_0 = -Q/2h$ . Using that  $||w||_h < \infty$ , yields

$$\frac{d}{dt}||w||_{h}^{2} = (m-1)\overline{w}_{0}^{(1)}w_{1}^{(1)} + (m+1)\overline{w}_{0}^{(2)}w_{1}^{(2)} + (w,F)_{h} + (F,w)_{h}.$$
(24)

By using the boundary conditions (20c) equation (24) is reduced to

$$\frac{d}{dt}||w||_{h}^{2} = -|(m-1)||w_{0}^{(1)}|^{2} - |(m+1)||w_{0}^{(2)}|^{2} + (w,F)_{h} + (F,w)_{h}.$$
(25)

To continue, we first assume that F = 0 in equation (25) and integrate,

$$||w(t)||_{h}^{2} + \int_{0}^{t} (|(m-1)| |w_{0}^{(1)}|^{2} + |(m+1)| |w_{0}^{(2)}|^{2}) d\tau \le ||f||_{h}^{2}.$$
 (26)

From the boundary conditions we have that

$$\int_0^t |w_0|^2 d\tau = \int_0^t |w_1|^2 d\tau.$$

This together with equation (26) give us the estimate

$$\min(|m-1|, |m+1|) \int_0^t |w_i|^2 d\tau \le ||f||_h^2, \quad i = 0, 1.$$

Since |m| < 1 we have the estimate

$$||w(t)||_{h}^{2} + C \int_{0}^{t} (|w_{0}|^{2} + |w_{1}|^{2}) d\tau \le 2||f||_{h}^{2}, \tag{27}$$

where C>0 is a constant. By Duhamel's principle we finally have

$$||w(t)||_h^2 + C \int_0^t (|w_0|^2 + |w_1|^2) d\tau \le 2||f||_h^2 + 2 \int_0^t ||F(\tau)||_h^2 d\tau.$$

Г

Consider (21). By the energy method,

$$\frac{d}{dt}||y||_h^2 \le C_1(|y_0|^2 + |y_1|^2) \quad C_1 > 0, \text{ constant.}$$
(28)

We will use Laplace transform technique to derive an estimate for the right hand side of (28). First Laplace transform (21) in time, yielding

$$2sh\hat{y}_i = Q\hat{y}_i,\tag{29a}$$

$$LS\hat{y}_0 = \hat{G}, \quad ||\hat{y}||_h < \infty. \tag{29b}$$

We need to estimate the solution for all Re  $(\tilde{s}) > 0$ ,  $\tilde{s} = sh$ .

Equation (29a) is a system of two uncoupled difference equations

$$z_{i+1} + \frac{2\tilde{s}}{\lambda_k} z_i - z_{i-1} = 0, (30)$$

with  $\lambda_1 = m - 1$  and  $\lambda_2 = m + 1$ . With the ansatz  $z_i = c\kappa^i$  we get

$$\kappa^2 + \frac{2\tilde{s}}{\lambda_k}\kappa - 1 = 0 \tag{31}$$

with the solutions

$$\kappa_{1,2} = -\frac{\tilde{s}}{\lambda_k} \pm \sqrt{\left(\frac{\tilde{s}}{\lambda_k}\right)^2 + 1} \tag{32}$$

From (31) we know that  $\kappa_1 \kappa_2 = -1$ . For Re  $(\tilde{s}) > 0$  there will alway be exactly one of  $\kappa_1$  and  $\kappa_2$  with  $|\kappa| < 1$ . Call this root  $\sigma_k$ . Hence  $\sigma_k$  is defined by

$$\sigma_k(\tilde{s}) = -\frac{\tilde{s}}{\lambda_k} - \sqrt{\left(\frac{\tilde{s}}{\lambda_k}\right)^2 + 1} \quad \text{if } \lambda_k < 0$$
 (33a)

$$\sigma_k(\tilde{s}) = -\frac{\tilde{s}}{\lambda_k} + \sqrt{\left(\frac{\tilde{s}}{\lambda_k}\right)^2 + 1} \quad \text{if } \lambda_k > 0.$$
 (33b)

The general solution of equation (29a) can be written as

$$\hat{y}_i = \begin{pmatrix} \sigma_1^i & 0\\ 0 & \sigma_2^i \end{pmatrix} \mathbf{c}. \tag{34}$$

The boundary condition (29b) yields

$$H(\tilde{s})\mathbf{c} = \hat{\tilde{G}}.\tag{35}$$

where

$$H(\tilde{s}) = LS \begin{pmatrix} \sigma_1(\tilde{s}) & 0\\ 0 & \sigma_2(\tilde{s}) \end{pmatrix}. \tag{36}$$

If  $|(H(\tilde{s}))^{-1}| \leq C$  for all Re  $(\tilde{s}) \geq 0$  then (35) has a solution such that

$$|\hat{y}_j|^2 \le K_j |\hat{\hat{G}}|^2$$
, Re  $(\tilde{s}) > 0$ ,  $j = 0, 1$ , (37)

where the constant  $K_j$  is independent of  $\tilde{s}$  and  $\hat{\tilde{G}}$ .

By Parseval's relation,

$$\int_0^\infty e^{-2\eta\tau} |y_j(\tau)|^2 d\tau \le K_j \int_0^\infty e^{-2\eta\tau} |\tilde{G}(\tau)|^2 d\tau \le K_j \int_0^\infty |\tilde{G}(\tau)|^2 d\tau, \quad \eta > 0.$$
(38)

Since the right-hand side is independent of  $\eta$  and  $y_j(\tau)$  for  $0 \le \tau \le t$  does not depend on  $\tilde{G}(\tau)$  for  $\tau > t$ , it follows that

$$\int_{0}^{t} |y_{j}|^{2} d\tau \le K_{j} \int_{0}^{t} |\tilde{G}(\tau)|^{2} d\tau. \tag{39}$$

If we integrate equation (28) and use the estimate (39) for the boundary terms we get

$$||y(t)||_h^2 \le C_1(K_0 + K_1) \int_0^t |\tilde{G}(\tau)|^2 d\tau.$$
 (40)

This completes the proof of the following lemma.

**Lemma 2** If  $|(H(\tilde{s}))^{-1}| \leq C$  for all Re  $(\tilde{s}) \geq 0$  then the solution of (21) satisfies

$$||y(t)||_h^2 \le K \int_0^t |\tilde{G}(\tau)|^2 d\tau, \quad K > 0, \ constant.$$
 (41)

By combining lemma (1) and lemma (2) we obtain the following theorem.

**Theorem 1** Assume that the boundary conditions can be expressed as in (22). If  $|(H(\tilde{s}))^{-1}| \leq C$  for all Re  $(\tilde{s}) \geq 0$  then the problem (19) is strongly stable, i.e. the solution satisfies,

$$||v(t)||_{h}^{2} \le K\left(||f||_{h}^{2} + \int_{0}^{t} |G(\tau)|^{2} d\tau + \int_{0}^{t} ||F(t)||_{h}^{2} d\tau\right). \tag{42}$$

Here K is a constant independent of F, G and f.

Note that if  $\det(H(\tilde{s})) = 0$  for some  $\tilde{s}_0$  with Re  $(\tilde{s}_0) > 0$  then the problem cannot be stable in any sense. If Re  $(\tilde{s}_0) = 0$  then stability cannot be determined without further investigations, see [3].

#### 3.2 Extrapolation of Primitive Variable

In this and the following subsection we investigate whether the assumption in theorem 1 are satisfied for (19) with boundary conditions (12) and (14) respectively, i.e. if the boundary condition can be expressed as in (22) and if  $|(H(\tilde{s}))^{-1}| \leq C$  for all Re  $(\tilde{s}) \geq 0$ . In the two subsections we only consider Re  $(\tilde{s}) \geq 0$ .

Consider the boundary conditions with extrapolation of primitive variable, (12). This boundary condition can be expressed as in (22). We have

$$H(\tilde{s}) = \begin{pmatrix} -(1 - \sigma_1(\tilde{s}))^2 & (1 - \sigma_2(\tilde{s}))^2 \\ 1 + \sigma_1(\tilde{s}) & 1 + \sigma_2(\tilde{s}) \end{pmatrix}, \tag{43}$$

Hence,

$$H^{-1}(\tilde{s}) = \frac{1}{\det(H(\tilde{s}))} \begin{pmatrix} 1 + \sigma_2(\tilde{s}) & -(1 - \sigma_2(\tilde{s}))^2 \\ -(1 + \sigma_1(\tilde{s})) & -(1 - \sigma_1(\tilde{s}))^2 \end{pmatrix}, \tag{44}$$

where

$$\det H(\tilde{s}) = ((1 - \sigma_1(\tilde{s}))^2 (1 + \sigma_2(\tilde{s})) + (1 + \sigma_1(\tilde{s}))(1 - \sigma_2(\tilde{s}))^2. \tag{45}$$

We have

$$\lim_{|\tilde{s}| \to \infty} H^{-1}(\tilde{s}) = \frac{1}{2} \begin{pmatrix} 1 & -1 \\ -1 & -1 \end{pmatrix}$$
 (46)

Hence  $|(H(\tilde{s}))^{-1}| \leq C$  for all  $\tilde{s}$  iff  $\det H(\tilde{s}) \neq 0$  for all  $|\tilde{s}| \leq K$ .

To determine whether

$$\det H(\tilde{s}) = 0 \tag{47}$$

has any roots with Re  $(\tilde{s}) > 0$  we introduce the transformation

$$Z = \frac{\tilde{s}}{m+1}$$
 and  $B = \frac{1+m}{1-m}$ . (48)

We can express  $\sigma_1$  and  $\sigma_2$  in the new variables:

$$\sigma_1 = ZB - \sqrt{(ZB)^2 + 1},$$

$$\sigma_2 = -Z + \sqrt{Z^2 + 1}.$$
(49)

Hence, we also have

$$\sigma_1^2 = 1 + 2ZB\sigma_1, 
\sigma_2^2 = 1 - 2Z\sigma_2,$$
(50)

Introduction of (49) and (50) into (47) and some algebraic manipulations give

$$Z^{3}(c_{4}Z^{4} + c_{3}Z^{3} + c_{2}Z^{2} + c_{1}Z + c_{0}) = 0$$
(51)

where

$$c_4 = 4B^3(B-1), (52)$$

$$c_3 = B^2(B2 - 14B + 1), (53)$$

$$c_2 = 4B(B-1)(B^2 - 3B + 1), (54)$$

$$c_1 = -4B(3B^3 - 2B + 3), (55)$$

$$c_0 = -8(B-1)(B^2+1). (56)$$

By the manipulations of the equation, we have introduced new roots, which are not roots of the original equation. It is easy to see that no real  $\tilde{s}$  can solve (47). Hence, we are only interested in complex Z, so we study the complex roots of the fourth degree polynomial

$$c_4 Z^4 + c_3 Z^3 + c_2 Z^2 + c_1 Z + c_0 = 0. (57)$$

We have determined the roots numerically. The fourth degree polynomial will have two real and two complex conjugate roots. The complex roots of (57) are plotted in figure (1). By substituting the complex roots of (57) into (47)

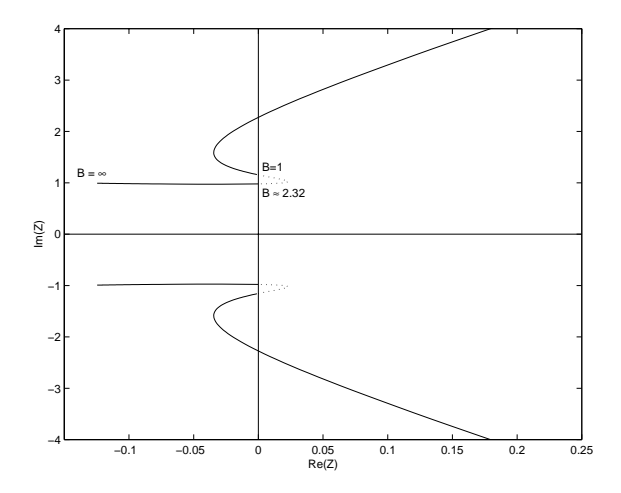


Figure 1: The complex roots of (57). The dotted part indicates solutions with Re  $(Z) \ge 0$  that correspond to solutions of (47) with Re  $(\tilde{s}) > 0$ .

we find that for B in the interval  $(1, B_1)$ ,  $B_1 \approx 2.32$ , there are two complex conjugate solutions of (47) with Re  $(\tilde{s}) \geq 0$ . For all other B-values there are no solutions with Re  $(\tilde{s}) \geq 0$ . Hence, for  $M \in (0, M_1)$ , with  $M_1 \approx 0.4$ , the problem is not stable.

#### 3.3 Extrapolation of Characteristic Variable

Consider the boundary conditions with extrapolation of the characteristic variable, (14). This boundary condition can also be expressed as in (22). We have

$$H(\tilde{s}) = \begin{pmatrix} -2(1-\sigma_1)^2 & 0\\ 1+\sigma_1 & 1+\sigma_2 \end{pmatrix}.$$
 (58)

Hence.

$$H^{-1}(\tilde{s}) = \frac{1}{\det(H(\tilde{s}))} \begin{pmatrix} 1 + \sigma_2 & 0\\ -(1 + \sigma_1) & -2(1 - \sigma_1)^2 \end{pmatrix}, \tag{59}$$

where

$$\det H(\tilde{s}) = -2(1 - \sigma_1)^2 (1 + \sigma_2). \tag{60}$$

We have

$$\lim_{|\bar{s}| \to \infty} H^{-1}(\tilde{s}) = \frac{1}{-2} \begin{pmatrix} 1 & 0 \\ -1 & -2 \end{pmatrix}$$
 (61)

For  $\tilde{s} \neq 0$ , we have  $|\sigma_k| < 1$ . For  $\tilde{s} = 0$ , we have  $\sigma_1 = -1$  and  $\sigma_2 = 1$ . Hence,  $\det H_2(\tilde{s}) \neq 0$  and the problem is strongly stable.

**Remark:** The above analysis is easily extended to the full system (4). A boundary condition for  $\rho$  must be added. If a condition that yields a strongly stable scalar problem is used, then the full system will be strongly stable.

#### 3.4 Order of Accuracy in Case 2

Consider (8) together with boundary condition (14). In the discretization of the continuous problem, we have used operators that are formally second order. This does not guarantee that the numerical solution is second order accurate. Hence the actual accuracy must be investigated.

Let  $v^*(x,t)$  denote the true solution. Then by Taylor expansion the error  $e_i(t) = v_i(t) - v^*(x_i,t)$  satisfies

$$\frac{de_i}{dt} = Qe_i + h^2 F_i(t), \quad i = 1, 2, \cdots, 
L_2 e_0 = h^2 g(t), \quad e_i(0) = 0.$$
(62)

If the initial condition and the boundary condition are smooth and compatible then F and g are smooth functions. The equations for the error  $e_i(t)$  is of the same form as the equations for  $v_i(t)$ . Hence, the equation for the error is strongly well-posed and the solution satisfies

$$||e(t)||_{h}^{2} \le h^{4}K\left(\int_{0}^{t} ||F(\tau)||_{h}^{2}d\tau + \int_{0}^{t} |g(\tau)|^{2}d\tau\right),$$
 (63)

where K is independent of F, g and t. Hence, the order of accuracy is two as expected.

# 4 Numerical experiments in one space dimension

In this section we verify the theoretical results experimentally and compare the effectiveness of the different numerical boundary conditions. Details of the applied difference approximations are found in 4.1. In 4.2 we give the parameters for our test cases and also account for the results.

#### 4.1 Description of the discretization

Two issues must be addressed before the analyzed semi-discrete problem can be turned into a complete numerical algorithm. First we must introduce a boundary to the right, we denote the x-interval [0, L]. Second, we have to discretize time.

Recall that the grid points are  $x_i = ih - h/2$ , we choose h so that L = Nh. This implies that we have N grid points in the interval [0, L] and the boundaries x = 0 and x = L lies centered between grid points. Our unknowns are  $\{(u_i, p_i)^T\}_{i=1}^N$ , where T denotes the transpose operation.

The semi-discrete approximation (8) consists of 2N coupled ODE's which contain  $(u_0, p_0)^T$  and  $(u_{N+1}, p_{N+1})^T$ . Counting the number of equations and unknowns we see that the numerical method requires two boundary conditions on each boundary to eliminate  $(u_0, p_0)^T$  and  $(u_{N+1}, p_{N+1})^T$ .

In the computations we will examine three versions of boundary conditions, described below. In all cases the discretization of the physical pressure boundary condition (9) is the same. In the computations the boundary conditions will be homogeneous:

$$p_0 + p_1 = 0$$
 and  $p_N + p_{N+1} = 0$ .

We use the initial data to get a non-trivial solution. For the remaining boundary conditions we examine three cases which we now list

Case 1. Here we use the extrapolation formula (11) for the primitive variable. This gives, for the two boundaries

$$u_0 - 2u_1 + u_2 = 0$$
  
$$u_{N-1} - 2u_N + u_{N+1} = 0.$$

We see directly how to express  $(u_0, p_0)^T$  and  $(u_{N+1}, p_{N+1})^T$  in terms of the unknowns at the "inner" points.

Case 2. In this case we apply the extrapolation formula to the outgoing characteristic variable, for the left boundary this gives equation (13). We use the pressure boundary condition to solve for the outer points and arrive at the expressions

$$u_0 = 2u_1 - 3p_1 - u_2 + p_2$$
  
$$u_{N+1} = 2u_N + 3p_N - u_{N-1} - p_{N-1}.$$

Case 3. The above two alternatives were introduced in section 2. In this section we also study a third case. This is derived by applying the simplest possible extrapolation of the outgoing characteristic variable. To the left we have

$$u_0 - p_0 = u_1 - p_1$$
.

To the right we have a corresponding expression. Using the pressure boundary condition we can solve for the outer points and get the expressions

$$u_0 = u_1 - 2p_1$$
  
$$u_{N+1} = u_N + 2p_N.$$

The purpose of investigating these boundary conditions is to show the need for more accurate extrapolations at the boundary because of the low accuracy for the overall method resulting from this discretization.

**Remark:** In the three cases above we use the same procedure to derive boundary conditions on both boundaries. A side effect of this is that we simultaneously investigate the effectiveness of the boundary condition on an inflow and an outflow boundary. This will be clearly seen for case 1, illustrated in figure 4.

**The time-discretization.** We use a fourth order Runge-Kutta method for the time stepping. The high accuracy should allow us to isolate the study of the space discretization. We denote the length of the time step k.

#### 4.2 Results

For the three test cases with different boundary conditions described above we determine the convergence rate by experiments with refinement of the grid. The following parameters are fixed in all computations.

- The length of the computational interval: L=2.
- The length of the time interval: T=4.
- The CFL-number:  $\frac{k}{h} = 1$ .
- The "Mach"-number: m = 0.25

The parameter m is negative if the constant flow we linearize at goes to the left, so |m| is the Mach-number. The initial data is also the same, we construct it using the function

$$\phi(x) = \begin{cases} e^{-1/x^2}, & x > 0 \\ 0, & x \le 0 \end{cases}$$

which is smooth and has supp  $\phi = [0, \infty)$ . This function is used for the cut-off near the boundaries and we have the following form of the initial data

$$\begin{cases} u(x,0) = \phi(\alpha x)\phi(\alpha(x-L))f_0(x) \\ p(x,0) = 0. \end{cases}$$

Here  $\alpha$  is chosen to  $\sqrt{5}$  in the experiments, and we use  $f_0(x) = \sin(5x)$ . The initial data is shown in figure 2. In figure 3 we show the solution at time t = 4 computed using the second boundary condition and a very fine grid.

Case 1. According to the theory, the boundary conditions at x=0, the inflow boundary, will cause instability for this value of m. The same boundary condition at the right boundary is stable. We illustrate this behavior in figure 4 where we show the solution at t=1.16. We have N=500. We stop the time stepping when the "blow-up" is apparent and before it has affected the solution in the right part of the computational interval. In the same figure we have for comparison, plotted the converged solution computed with the boundary conditions of case 2 and a more refined grid.

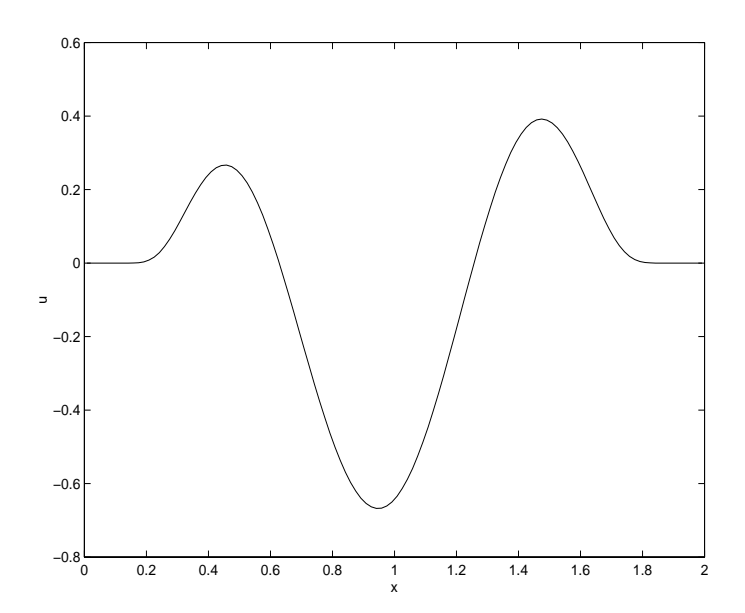


Figure 2: Initial data for u. The initial data for the pressure is p(x,0)=0.

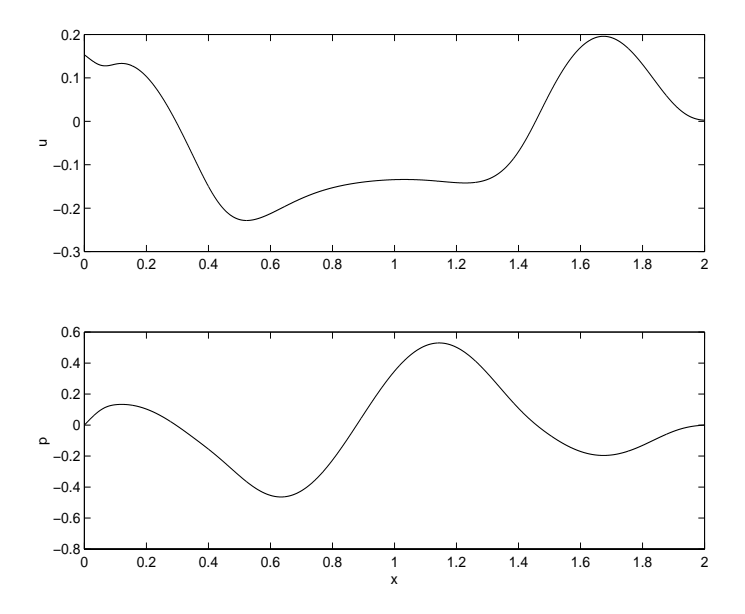


Figure 3: The solution at time t=4. The solution is computed using the boundary conditions of case 2 and a very fine grid.

Case 2. Here we give numerical evidence of the second order accuracy predicted by theory. We investigate this case by first discretizing with N=180. Then we refine by successively increasing N with a factor three, we compute with N=540, N=1620 and N=4820. The points

$$x_n = n\Delta x - \Delta x/2,$$
  $n = 1, 2, \dots, 20$   $\Delta x = 0.1$  (64)

then lie on grid points for our choice of N-values. We compare the different computed solutions in these points at time t=4. We choose this time level to ensure that the solution has been reflected in both boundaries. The propagation speed to the right is 1.25 length units/time unit and the speed to the left is 0.75 l.u/t.u . To determine the order of accuracy we use that

$$u_i^{(h)} \approx u_{exact}(x_i) + Ch^q$$
.

Combining three solutions we can thus solve for q. We use discrete  $L^2$ -norms

$$q_{exp} = \frac{1}{\ln 3} \ln \frac{\|u^{(h)} - u^{(h)}\|}{\|u^{(h/3)} - u^{(h/9)}\|}$$
 (65)

where we use the 20 points introduced above to define the norm

$$||u||^2 = \Delta x \sum_{n=1}^{20} |u_{i(n)}|^2.$$

Here  $\Delta x = L/20$  and i(n) indicate that we take points with the same x-coordinate, and thus different i, when we refine. Our choice of test runs give two values of  $q_{exp}$ , these are given in table 4.2 where we also summarize the results for the less accurate approximation of case 3.

A presentation of the computed solutions is shown in figure 5 where u(x,4) is plotted. The full line is the computation with N=4860. The coarser grids are shown by symbols at the 20 x-values we used for the norm comparison above. The crosses represent the solution with N=1620, the rings: N=540 and the diamonds: N=180.

Case 3. As mentioned above, this case is include to show the need for the more accurate approximations of case 1 and 2. The computations here are thus designed to verify the first order accuracy of the overall scheme in this case. Just as for the second boundary condition we use the refinement N=180,540,1620,4860. The resulting two values of  $q_{exp}$  are given in table 4.2. There we see that the value of  $q_{exp}$  determined by the coarser grids is not very close to one. This indicates that this scheme is not in the asymptotic region of convergence for N=180.

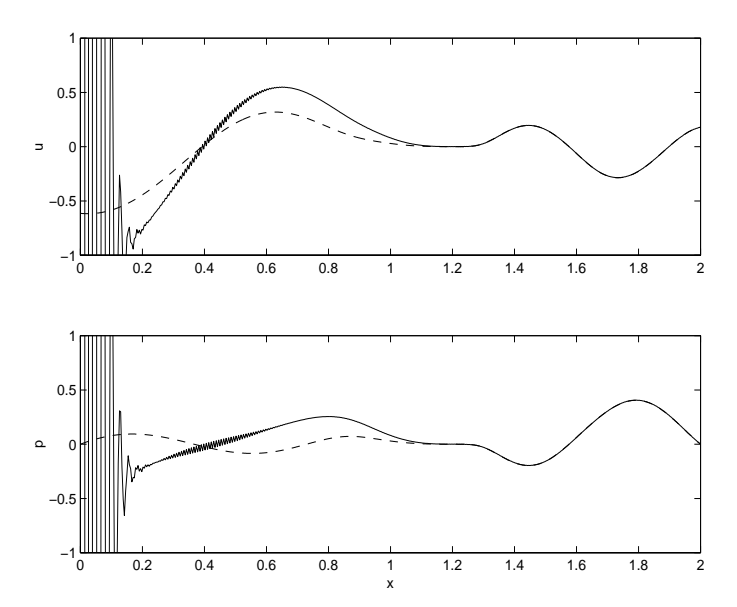


Figure 4: Blow-up at the boundary, t=1.16. Here we see that the boundary conditions of case 1 gives an unstable difference scheme at an inflow boundary, while the numerical solution at the outflow boundary is stable. The full line is computed with the boundary conditions of case 1 as described above. The dashed line is the converged solution computed with the boundary conditions of case 2 with N=1620.

	Test cases	
N-values used	2	3
{180,540,1620}	1.969	1.2428
{540,1620,4860}	2.018	0.9903
	'	

Table 1: The experimental order of accuracy  $q_{exp}$  defined by formula (65). The column "N-values used" indicates which computed solutions we insert in formula (65). In test case 2 we see a good agreement with second order accuracy. In test case 3 the first value is not very close to one. This indicates that, for this scheme, the N-values {180,540,1620} are not large enough to ensure that we get the asymptotic convergence rate.

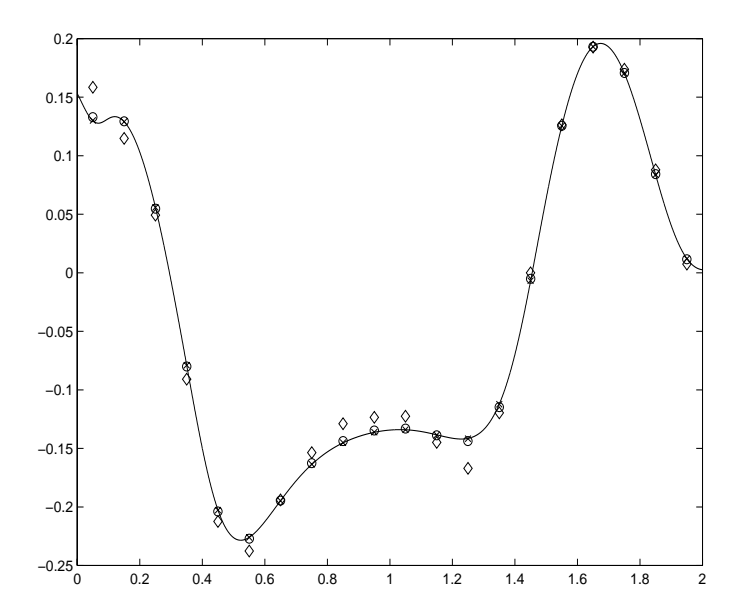


Figure 5: Convergence of the solution in case 2. The full line is the solution at time t=4 computed with N=4860. The crosses represent the solution with N=1620, the rings: N=540 and the diamonds: N=180. The last three solutions are shown in the gridpoints given by the expression (64).

### References

- B. Gustafsson. The Convergence Rate for Difference Approximations to Mixed Initial Boundary Value Problems. Math. Comp., 29:396-406, 1975.
- [2] B. Gustafsson. The Convergence Rate for Difference Approximations to General Mixed Initial Boundary Value Problems. SIAM J. Numer. Anal., 18(2), 1981.
- [3] Bertil Gustafsson, Heinz-Otto Kreiss, and Joseph Oliger. Time Dependent Problems and Difference Methods. John Wiley and Sons, INC, 1993.
- [4] T. Hagström and J. Nordström. Analysis of Extrapolation Boundary Conditions for the Linearized Euler Equations. In preparation.
- [5] N. Lindberg, G. Efraimsson, and J. Nordström. Numerical Investigation of Extrapolation Boundary Conditions for the Euler Equations. Technical report, FFA, Stockholm, 1998. FFA TN 1998-03.
- [6] S. Meijer, I.A. Lindblad, and S. Wallin. Acoustic prediction for transonic propellers including nonlinear near-field effects. In *Proceedings from the 14th DGLR/AIAA Aeroacoustics Conference*, number 92-020-66, 1992.
- [7] A. Rizzi, P. Eliasson, I. Lindblad, C. Hirsch, C. Lacor, and J. Hauser. The Engineering of Multiblock Multigrid Software for Navier-Stokes Flows on Structured Meshes. *Computers and Fluids*, 22:357–372, 1995.